New Insight into Mechanism of Cr(VI) Migration and Transformation in Typical Soils of Chromite ore Processing Residue (COPR) Contaminated Sites

Minghai Wei
Chinese Academy for Environmental Planning
Wenting Li
Geological Survey of Jiangsu Province
Jie Tang
China University of Geosciences Beijing
Jia Zhang (zjia@cugb.edu.cn)
China University of Geosciences, Beijing
Honghan Chen
China University of Geosciences Beijing

Research Article

Keywords: Chromite ore processing residue (COPR), Cr(VI), soil, risk, remediation

Posted Date: May 21st, 2021

DOI: https://doi.org/10.21203/rs.3.rs-439433/v1

New insight into mechanism of Cr(VI) migration and transformation in typical soils of chromite ore processing residue (COPR) contaminated sites

Minghai Wei[1,3], Wenting Li[1,2], Jie Tang[1], Jia Zhang[1,*], Honghan Chen[1]

[1] *Beijing Key Laboratory of Water Resources and Environmental Engineering, China University of Geosciences, Beijing 100083, China*

[2] *Geological Survey of Jiangsu Province, Nanjing 210018, China*

[3] *Chinese Academy of Environmental Planning, Beijing 100012, China*

——Submit to *Environmental Earth Sciences*

Corresponding author:

Jia Zhang

Beijing Key laboratory of Water Resources and Environmental Engineering, China University of Geosciences, Beijing 100083, P. R. China

E-mail: zjia@cugb.edu.cn

Abstract

Chromite ore processing residue (COPR) storage sites are widely distributed all over the world, causing serious soil and groundwater pollution. However, the differences in soil constituents and properties between different regions are significant, and the dynamic migration and transformation of Cr(VI) in different types of soil under alkaline condition of the COPR site is still unclear. In this study, the typical black soil, red soil and loess in different regions of China were chosen to investigate the adsorption kinetics and thermodynamics of Cr(VI) under the original pH conditions of the soil, and then the alkaline Cr(VI) solution was introduced into the soil column to simulate the dynamic migration and transformation process of Cr(VI) at COPR sites. According to the results, the Cr(VI) breakthrough curve predicted by the solid-liquid distribution coefficient K_d based on the static isotherm adsorption experiments significantly underestimated and overestimated the retention effect of black soil and red soil on Cr(VI) dynamic migration, respectively. For the black soil, the retention of Cr(VI) was dominated by Cr(VI) reduction, which is a slow reaction compared with Cr(VI) adsorption. Therefore, the reduction kinetics process during the column experiment cannot be neglected. In respect to the red soil, the outlet Cr(VI) concentration turned to be higher than the inlet concentration with the soil alkalization, which indicated that the adsorbed Cr(VI) desorbed again, and this is the main reason for the overestimation of Cr(VI) retention effect by the red soil. This study shows that the environmental risks of Cr in different types of soil are quite different, mainly related to the valence and occurrence form of Cr that governed by the soil constituents and properties. In addition,

the stable form of Cr in the black soil column after the reaction indicates that the soil organic matter can be used as a potential environmentally friendly remediation material for Cr(VI) contaminated soils at COPR sites.

Keywords: Chromite ore processing residue (COPR), Cr(VI), soil, risk, remediation.

1 Introduction

Chromium salt is an important chemical raw material widely used in electroplating, tanning, metallurgy, ceramics, dyes and wood preservation (Dhal et al. 2013). However, it is worth noting that hexavalent chromium (Cr(VI)) has potential cancer risk and is listed as one of the priority control heavy metal pollutants by USEPA Superfund (Saha et al. 2011). In the past few decades, the high lime roasting technology used in the production of chromium salts has produced a large amount of chromite ore processing residue (COPR), and many COPR storage sites have been formed worldwide. About 0.04%-2.59% (w:w) of Cr(VI) remains in the COPR, and since a large amount of alkaline substances such as calcium carbonate remain, the COPR tends to exhibit a strong basic character (Chrysochoou et al. 2009; Foeldi et al. 2013). Cr(VI) exists in the form of CrO_4^{2-} under alkaline conditions and has strong mobility (Benjamin 2002; Zhang et al. 2018c). It is easy to infiltrate into the groundwater with the leaching filtrate of the precipitation, and spread to the downstream.

China is the largest amount of Cr slag produced country (Gao and Xia 2011). Since 1958, 63 chromium salt production plants have been built, covering 23 provinces, municipalities and autonomous regions, involving a variety of soil types, including black soil in the northeast, loess in the Loess Plateau and red clay in the southwest. The accumulated amount of Cr slag over a span of 30 years was more than 6 million tons (Wang et al. 2009). The soil and groundwater around the COPR storage site are generally heavily contaminated, which has become a secondary pollution source that continues to pose a threat to the surrounding ecological environment and human health

(Wang et al. 2011).

The migration and transformation process of Cr(VI) in soils is mainly controlled by adsorption/desorption, oxidization/reduction and dissolution/precipitation (Fonseca et al. 2009; Jardine et al. 1999). Cr(VI) will be reduced to Cr(III) when soil organic matter, S(II) and Fe(II) exist (Fendorf 1995). The generated Cr(III) can be complexed by soil organic functionalities or directly form hydroxide precipitation (Zhang et al. 2017; Zhang et al. 2018a). The mobility of Cr(III) in soil is generally poor, but migration also occurs under conditions of low soil pH or forming complexes with dissolved organic matter (DOM) (Weng et al. 1994). In addition, when MnO_2 minerals are present in the soil and the organic matter content is low, Cr(III) may also be oxidized to Cr(VI) (Landrot et al. 2012a; Landrot et al. 2012b). The retention process of Cr(VI) migration in soil involves both specific adsorption and non-specific adsorption. Non-specific adsorption can be taken as electrostatic adsorption. The specific adsorption mainly refers to the ligand exchange reaction between Cr(VI) and the surface ligand of soil particles. The common ligands include soil humus functionalities and iron oxyhydroxide surface hydroxylic groups (Jiang et al. 2008).

The migration and transformation processes of Cr(VI) in soil is closely related to soil material composition and physicochemical properties (Kožuh et al. 2000; Zhang et al. 2019a). The inorganic minerals in the soil have different degrees of adsorption and reduction on Cr(VI). Iron oxyhydroxides, such as hematite, goethite and ferrihydrite, have a strong adsorption effect on Cr(VI) at an acidic condition, which mainly form inner-sphere complexes (Johnston and Chrysochoou 2012; Johnston and Chrysochoou

2014; Xie et al. 2015). On the contrary, the adsorption of Cr(VI) by aluminum oxides, such as boehmite and gibbsite, is mainly dominated by outer-sphere complexes by electrostatic attraction adsorption and ion exchange adsorption (Johnston and Chrysochoou 2015; Johnston and Chrysochoou 2016). When Fe(II) is contained in the iron oxide, the iron oxide has a reducing ability on Cr(VI), such as magnetite (He and Traina 2005; Jiang et al. 2014). Cr(VI) anions are generally weakly adsorbed on clay minerals because the surface is usually negatively charged (Bradl 2004).

Soil organic matter has a significant retention effect on the migration of Cr(VI). This is because the surface of soil organic matter contains a large number of reactive functional groups, which can complex with Cr(VI) or reduce Cr(VI) into Cr(III). Dissolved organic matter can reduce Cr(VI) at low pH, and the removal efficiency of greatly decreased with the increasing pH (Gong et al. 2015). Dissolved organic matter can also form water-soluble complexes with Cr(VI) and Cr(III) to enhance their mobility (Weng et al. 2002). The undissolved organic matter can provide active sites for the adsorption of Cr(VI) and electrons for the reduction of Cr(VI), which plays a major role in the retention of Cr(VI) migration (Barnie et al. 2018; Zhang et al. 2019b; Zhang et al. 2018b). In addition, pH also has an important influence on the migration of Cr(VI). Generally, the lower pH is better for the reduction and adsorption of Cr(VI) (James and Bartlett 1983).

It is worth noting that different types of soil have various components. And the retention effects on Cr(VI) migration are significantly different (Fernandez-Pazos et al. 2013; Lee et al. 1999). However, the retention effects of the typical soils in China on

Cr(VI) migration in the COPR sites have not been reported yet. It had been proven that water in contact with COPR had a pH of 11-12, and could contain high concentration of Cr(VI) as the highly mobile and toxic anion chromate (Geelhoed et al. 2003). The migration and transformation of Cr(VI) in soil under hyperalkaline condition may be quite different from the neutral or acidic conditions. In this study, the black soil, red soil and loess from different areas of China were chosen to investigate the dynamic transportation and transformation of Cr(VI) in typical soils under extremely basic condition of COPR site, and the variation of Cr speciation in soils were investigated as well. This study will contribute to the development of Cr(VI) ecological risk assessment and remediation schemes design for COPR sites.

2 Materials and methods

2.1 Soil samples

In order to explore the migration and transformation characteristics of Cr(VI) in the typical black soil area, red soil area and loess area in China, the black soil of Antu City, Jilin Province (42°57′ 54″ N, 128°41′ 27″ E), the red soil of Qujing City, Yunnan Province(24°59′ 57″ N, 103° 36′ 21″ E), and the loess of Shangluo City, Shanxi Province(33°29′ 41″ N, 110°52′ 15″ E) were collected as the experimental soil samples. And these soil samples are all background soils about 500 meters away from the contaminated sites. When collecting soil samples, the areas with little human activity were tried to select. The surface vegetation was removed and soil within 30 cm below the surface was collected. After removing the crushed stone, plant debris and other impurities in the soil samples, the soil samples were naturally air-dried. Then, the

soil sample was ground and sieved to less than 0.25 mm in diameter, and stored in a dry and cool place for later use.

The chemical compositions of the soil samples were determined by X-ray fluorescence (XRF) using a Rigaku ZSX Primus spectrometer. The soil organic matter contents of the soil samples were determined by the muffle furnace method (Klingenfuss et al. 2014). And the soil samples were heated at 550 °C for 4 h. X-ray diffraction (XRD) patterns were obtained in a Rigaku D/max-RA powder diffraction-meter, which was used to determine the mineral compositions and clay mineral compositions of the soil samples. The point of zero charge (PZC) of the soil samples were determined by the salt titration method (Sijin et al. 2006). The pH of the soil samples were measured in water and 0.01M $CaCl_2$ at a soil/solution ratio of 1: 2.5 using a pH meter (Sartourius, PB-10) after calibration (Choppala et al. 2013).

2.2 Adsorption kinetics and thermodynamic experiment

The adsorption kinetics experiment was carried out in a 50 mL polyethylene centrifuge tube. A Cr(VI) stock solution (1000.0 mg/L) was prepared by adding 2.829 g dried potassium dichromate ($K_2Cr_2O_7$) into 1 L of deionized water and then stored at 4℃. The Cr(VI) solution (10.0 mg/L) was prepared by further diluting the stock solution using deionized water. 1 g of black soil, red soil and loess samples were added, separately. Then 30 mL of 10 mg L^{-1} Cr(VI) solution was added. 0.02 M NaCl was used as the supporting electrolyte to simulate the ion strength in actual groundwater. The initial pH was not adjusted, which was in accord with the pH of the deionized water (about 6.5). The tubes were placed in a constant temperature shaker at 25 °C, 175 rpm

for horizontal shaking. The samples were taken out at regular intervals, and the maximum reaction time was 24 h. The tubes were centrifuged at 3000 rpm for 10 min, and the supernatant was passed through a 0.45 μm filter. The pH of the filtrate was measured, and the concentration of Cr(VI) in the filtrate was determined by UV-vis spectrophotometer (SHIMADZU UV-1800). Then, the adsorption quantity of Cr(VI) by the soil sample was calculated according to the decreasing Cr(VI) concentration in solution. The experimental group set up three parallel samples with 0.02M NaCl background electrolyte. The blank sample was designed without Cr(VI), and the control sample was designed without soil samples. The Cr(VI) adsorption thermodynamics experiment was consistent with the adsorption kinetics experiment, except that the samples were taken out after shaking of 24 h and the initial concentrations of Cr(VI) were set to 5-50 mg L^{-1}. Experiment on the effect of pH on adsorption of Cr(VI) by soil was consistent with the adsorption kinetics experiment, except that the samples were taken out after shaking of 24 h and the initial pH values of Cr(VI) solution were set to 2-12.

2.3 Adsorption kinetics and isotherm model analysis

The pseudo first-order and pseudo second-order kinetic equations were utilized to analyze the kinetic experiment data. The pseudo first-order kinetic equation is derived from the equation $\frac{dc}{dt} = -k_1(c - c_e)$ (Moussout et al. 2018). It is shown as follows:

$$q_t = \frac{(C_0-(C_0-C_e)e^{-k_1 t}-C_e)V}{m} \quad (1)$$

where, q_t represents the Cr(VI) adsorption quantity on the soil samples. C_0 and C_e represent the initial concentration and equilibrium concentration of Cr(VI) in the

solution, respectively. k_1 represents the pseudo first-order kinetic constant. V and m represent the volume of the solution and mass of the soil sample, respectively.

The pseudo second-order kinetic equation is derived from the equation $\frac{dc}{dt} = -k_2(c - c_e)^2$ (Moussout et al. 2018). It is shown as follows:

$$q_t = \frac{(C_0 - \frac{C_0 - C_e}{1 + k_2 t(C_0 - C_e)} - C_e)V}{m} \quad (2)$$

where, k_2 represents the pseudo second-order kinetic constant. The meanings of the other parameters are consistent with Equation (1).

The Langmuir and Freundlich isotherm equations were utilized to analyze the thermodynamic experiment data, and the Langmuir isotherm equation is shown as follows:

$$q_s = \frac{q_m K_L C_e}{1 + K_L C_e} \quad (3)$$

where, q_s represents the Cr(VI) adsorption quantity on the soil samples. q_m represents the maximum Cr(VI) adsorption quantity on the soil samples. C_e represents the equilibrium Cr(VI) concentration in solution. K_L represents the Langmuir non-linear solid-liquid partition coefficient.

The Freundlich isotherm equation is shown as follows:

$$q_s = K_F {C_e}^n \quad (4)$$

where, the K_F represents the Freundlich non-linear solid-liquid partition coefficient. The meanings of the other parameters are consistent with Equation (3).

2.4 Column experiment of Cr(VI) dynamic transportation

Column experiment was conducted using three parallel plexiglass columns (3.5 cm in internal diameter; 22 cm height). The columns were filled with 2 cm of glass beads,

2 cm of quartz sand, 15 cm of soil (There were separate soil columns for black soil, red soil and loess), 1 cm of quartz sand and 2 cm of glass beads from bottom to top (Figure S1). The dry heap method was adopted for packing the soils into the column. That is, for the same soil, when every time the same mass of the soil was loaded, the soil was filled evenly to the same height. The sampling ports were positioned at a distance of 9 cm and 14 cm from the bottom of each column. The samples were collected at regular time intervals. Since the inner wall of the plexiglass column was relatively smooth, it was abraded by a sandpaper with a particle size of 25 μm before filling the medium in order to avoid preferential flow along the inner wall. In all the columns, the solution was loaded in an upflow mode using an adjustable multiport peristaltic pump set (Longer Precision Pump Co., Ltd., BT 100-1F). The pore volume was quantified by measuring the deionized water used to saturate the column. Furthermore, this value was used to calculate the porosity considering the given geometry of the column (Knorr et al. 2016). The porosity of each column and the weight of soil filled in each column are shown in Table S1. The bulk density was calculated by dividing the mass of soil packed into the column by the volume of soil portion in column.

To illustrate the convection-dispersion process of Cr(VI) in the soil columns, a breakthrough experiment was performed using Cl^-. That is, 0.02 M NaCl solution was loaded from the bottom to top. Cl^- is generally considered as a conservative tracer, which can be used to indicate the convection-dispersion process of Cr(VI) in the soil column. The program CXTFIT (Toride et al. 1995), a nonlinear least squares algorithm, was applied to the experimental results to determine solute transport parameters for the

columns. The actual flow velocity v and the diffusion coefficient D of each soil column were obtained, and the results are shown in Table S5.

In order to simulate the actual pH conditions of the leaching solution of the COPR site, 100 mg L^{-1} Cr(VI) solution with pH 11.5 and 0.02M NaCl background electrolyte was introduced into the soil column. And samples were taken out at two sampling ports and outlet holes at regular intervals. The concentration of Cr(VI) in the liquid phase was measured by UV-vis spectrophotometry, and the change in pH was measured. The data of X-ray photoelectron spectroscopy (XPS) obtained by a Kratos Axis Ultra X-ray photoelectron spectrometer were used to characterize the valence of Cr on the soil surface before and after the experiment.

2.5 Speciation analysis of Cr in the soil samples

In order to find out the changes of Cr content and speciation in the soil column before and after the reaction, the modified BCR sequential extraction method was used to study the unreacted soil and the soil samples at 0-5, 5-10 and 10-15 cm in the post-reaction soil column (Žemberyová et al. 2006). The modified BCR sequential extraction method divides the heavy metal form into water-soluble state, weak acid extractable state, reducible state, oxidizable state and residual state. The specific meaning of each form and the extraction reagents and procedures are shown in Table S2.

2.6 Convection-dispersion-reaction equation modeling

Based on the convection-dispersion equation, the CXTFIT program was used to fit the Cl^- ion and Cr(VI) breakthrough curves in soil column experiments. The convection-dispersion equation is as follows:

$$R\frac{\partial C}{\partial t} = \frac{\partial}{\partial Z}\left(D\frac{\partial C}{\partial Z}\right) - \frac{\partial}{\partial Z}(vC) + \frac{q_s}{\theta}C_s \quad (5)$$

$$R = 1 + \frac{\rho_b K_d}{\theta} \quad (6)$$

where, C represents the concentration of the solutes. D represents the dispersion coefficient. v represents the actual velocity. q_s and C_s are the flux and solute concentration at the input and output, which represent the boundary conditions. R represents the retardation factor. θ represents the porosity. ρ_b represents the bulk density of the soil samples. K_d represents the solid-liquid distribution coefficient.

3 Results and discussion

3.1 Characterization of the soil samples

The characterizations of the three soil samples are shown in Table 1. It can be found that the content of SiO_2 in the red soil sample is lower compared with the other soil samples. But the red soil contains higher content of Al_2O_3 and Fe_2O_3. Mineral composition analysis verified this point. Clay minerals account for about 55% of the mass in red soil, and kaolinite is the main clay mineral. The iron mineral content is about 7% in red soil, mainly composed of hematite. The major clay mineral in black soil and loess is andreattite. The CaO content in loess is high and the mineral composition analysis demonstrated that there was about 15% of calcite in loess. Additionally, organic matter content reaches 13.8% in black soil, while the organic matter content in red soil and loess is lower, only accounting for 0.47% and 0.63%, respectively.

The black soil and red soil samples belong to acidic soils with pH of 4.77 and 5.06, respectively, while the loess is alkaline soil with pH of 8.07. The acidity of the black

soil is related to its high organic matter content (Dai 2009). Organic matter contains a large amount of acidic functional groups (Zhang et al. 2018a) and possibly release a large number of protons. Red soil is the main agrotype in Southwest China, it is rich in iron, aluminum oxide with strong acidity and high consistency (Ma et al. 2013). The alkalinity exhibited by the loess is mainly related to its higher calcite content. According to the determining results of PZC as shown in Figure S2, the PZC of black soil and red soil is lower, 3.67 and 4.29 respectively, and the PZC of loess is higher, 8.19. This is because the acidic functional groups rich in organic matter in black soil can provide a large amount of variable charge (Coleman et al. 1989), and the clay minerals rich in red soil have a large number of permanent negative charges through isomorphous substitution (Nakato et al. 2017). Additionally, the bulk density of black soil was 0.91 g cm^{-3}, which was quite lower compared with the red soil and loess (1.14 and 1.29 g cm^{-3}, respectively), and this is mainly related to the higher content of organic matter (Coleman et al. 1989).

Table 1. The physicochemical properties and chemical, mineral compositions of the black soil, red soil and loess samples.

Samples	Chemical composition (%)*				Particle size distribution (%)			OM (%)	Bulk density (g cm^{-3})	pH_{H2O}	PZC
	SiO_2	Al_2O_3	Fe_2O_3	CaO	Sand	Silt	Clay				
Black soil	51.21	18.39	3.17	1.68	84.94	14.11	0.95	13.80	0.91	4.77	3.67
Red soil	38.80	26.56	13.74	0.13	73.45	20.98	5.57	0.47	1.14	5.06	4.29
Loess	52.08	15.23	4.25	9.35	54.42	38.95	6.63	0.63	1.29	8.07	8.19

Samples	Mineral composition (%)#						Clay mineral composition (%)#				
	Quartz	Hematite	Anorthose	Microcline	Calcite	Clay minerals	Andreattite	Illite	Kaolinite	Chlorite	Roseite
Black soil	35	ND	30	11	ND	24	81	6	6	7	ND
Red soil	38	7	ND	ND	ND	55	ND	3	75	ND	14
Loess	35	ND	26	4	15	20	61	24	5	10	ND

* The chemical compositions determined by XRF were semi-quantitative. # The mineral compositions and clay mineral composition obtained from XRD were semi-quantitative. ND represents not detected.

3.2 Kinetic and thermodynamic experiments

In order to illustrate the adsorption characteristics of Cr(VI) in different soil samples, the adsorption kinetic experiments of Cr(VI) were carried out. And the results are shown in Figure 1. The experimental results show that the adsorption of Cr(VI) by red soil is stronger, while the adsorption of black soil is weaker, and the adsorption of Cr(VI) by loess is hardly observed. During Cr(VI) adsorption by the soil samples, the pH of the solutions kept almost unchanged (Figure S3).

The adsorption rate of Cr(VI) by red soil is faster, and it basically reaches equilibrium in about 4 h, and the maximum adsorption capacity is about 241.36 mg/kg. Since pH of the solution was above 5 during the reaction, which was higher than PZC of the red soil (PZC=4.29), the surface of the red soil was negatively charged. And there was electrostatic repulsion between the surface of the red soil and the Cr(VI) anion. Therefore, the electrostatic attraction was not likely to be the driving force of Cr(VI) adsorption on the surface of the red soil. In addition, considering that the adsorption of Cr(VI) by kaolinite is weak (Jin et al. 2014), the adsorption of Cr(VI) by hematite by ligand exchange may be the main driving force for its adsorption on red soil (Adegoke and Adekola 2012; Singh et al. 1993).

It is worth noting that the adsorption of Cr(VI) on black soil did not reach equilibrium at the end of the experiment, which is quite different from that of the red soil. The adsorption process can be divided into two stages, fast and slow. This is because the black soil followed the “adsorption-reduction” mechanism for the retention of Cr(VI) as reported by our previous research (Zhang et al. 2017), that is, Cr(VI) is

quickly adsorbed to the black soil surface, and the adsorbed Cr(VI) is reduced to Cr(III) by the reducing functional group in the soil organic matter (such as phenolic groups and hydroxylic groups), wherein the reduction process is a rate limiting step of the entire reaction (Zhang et al. 2019a). That is why the adsorption amount of Cr(VI) increases rapidly in the initial stage of the reaction and then rises slowly, which also indicates that the reduction reaction of Cr(VI) by black soil is still going on.

The results of the kinetic experiments were fitted using pseudo first-order and pseudo second-order reaction kinetic models, and the fitting results are shown in Figure 1(a) and Table S3. Since the obtained R^2 values were consistent and closer to unity for the pseudo-second order kinetic equation than for the pseudo-first order kinetic equation, the adsorption kinetics can be well described by the pseudo-second order kinetic equation. This indicates that the retention of Cr(VI) on three soil samples is related to both the Cr(VI) concentration and the number of adsorption reduction sites on the soil surface.

In order to reveal the thermodynamic characteristics of Cr(VI) adsorption of three soil samples, isothermal adsorption experiments were carried out. The results are shown in Figure 1(b). The adsorption of Cr(VI) by red soil is larger, and the adsorption of Cr(VI) by black soil is lower. The adsorption of Cr(VI) by loess is negligible, which is consistent with the results of the kinetic experiments. With the increase of Cr(VI) concentration, the growth trend of Cr(VI) adsorption quantities by black soil and red soil show nonlinear characteristics. The Freundlich isotherm adsorption models had better fitting performances on the experimental results (Fitting results are shown in

Table S4). According to the Freundlich model, the maximum adsorption capacity of black soil and red soil can reach 247.11 mg kg^{-1} and 869.45 mg kg^{-1}, respectively.

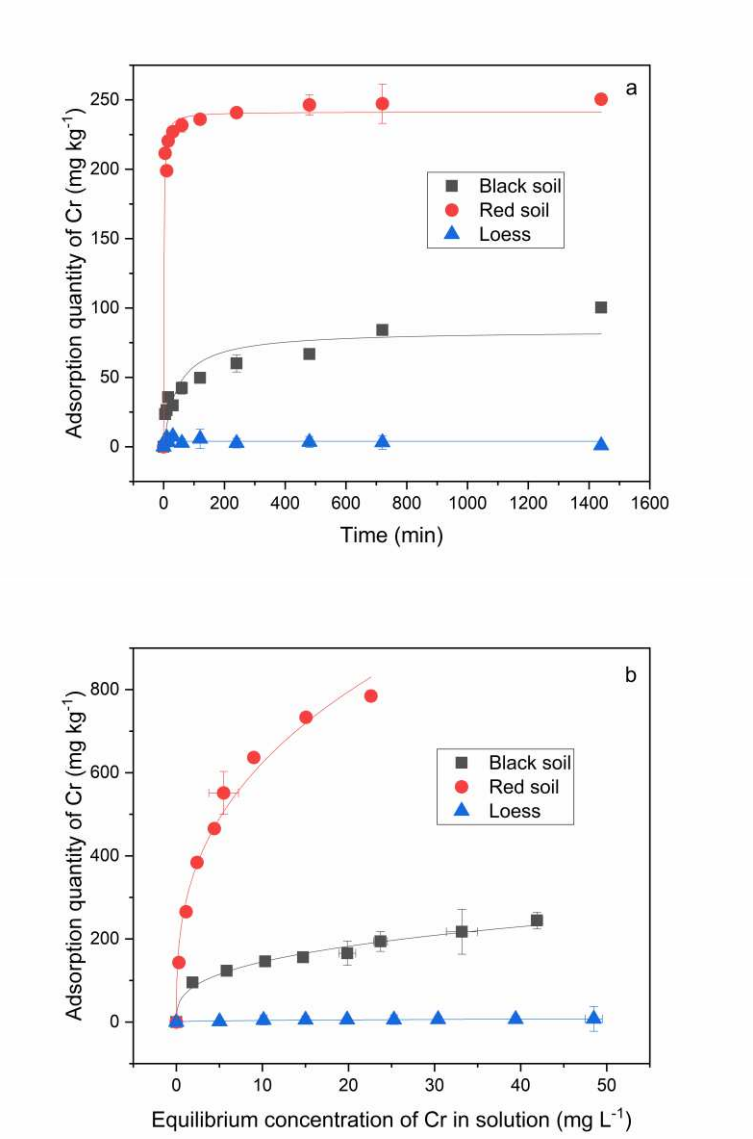

Figure 1. The (a) kinetic and (b) thermodynamic characteristics of Cr(VI) adsorption by black soil, red soil and loess samples at 25 °C. The initial pH of Cr(VI) solution was 6.5, and the background electrolyte was 0.02 M NaCl. The error bar represented Standard Error of Mean. In kinetic experiments, the simulation results were more consistent with the pseudo second-order reaction kinetic model. The solid lines are Freundlich isotherm in (b).

The effect of pH on the adsorption of Cr(VI) on the three soil samples is shown in Figure S4. As indicated, the adsorption of Cr(VI) by the red soil and black soil decreased with pH increasing. The adsorption amount of Cr(VI) by the loess is low, and it remains almost unchanged with pH increasing. The adsorption amount of Cr(VI) by red soil decreased rapidly between pH 5-7, while the adsorption amount of Cr(VI) by black soil decreased almost linearly with the increase of pH. In view of the fact that the PZC of hematite is about 7 (Estes et al. 2013), this further confirms that the adsorption of Cr(VI) by the red soil is mainly controlled by the ligand exchange between Cr(VI) and the surface hydroxyl groups of hematite. So the adsorption of Cr(VI) by the red soil is affected by the variable charge of the surface of hematite significantly. The adsorption of Cr(VI) by the black soil is mainly controlled by the reduction process, and the reduction is mainly restricted by the concentration of hydrogen ions (Huang et al. 2012), therefore, the adsorption amount of Cr(VI) by black soil gradually decreases with the increase of pH value.

3.3 Cr(VI) dynamic transport in the soil columns

In the loess column, the Cr(VI) breakthrough process was very fast, which was only slightly delayed compared with the Cl^-. This is consistent with the result of the weak adsorption of Cr(VI) on the loess observed in the kinetic and thermodynamic batch experiments. It is interesting to find that the black soil had a stronger retardation effect on Cr(VI) migration than that of the red soil in the column experiment. This is contrary to the results obtained in the batch experiments, wherein the adsorption capacity of red soil for Cr(VI) is much stronger than that of the black soil. The solid red line in Figure

2 represents the Cr(VI) breakthrough curve, which was simulated by the solid-liquid distribution coefficient K_d. By comparing the actual breakthrough curve of Cr(VI) with the simulated breakthrough curve of Cr(VI), it can be found that if the K_d is used to evaluate the retardation effect on Cr(VI) by soils in COPR contaminated sites, the effect of black soil will be significantly underestimated, and the adsorption capacity of red soil for Cr(VI) will be significantly overestimated.

As mentioned above, the black soil is rich in organic matter and the adsorption kinetic of Cr(VI) by black soil followed "adsorption-reduction" mechanism (Zhang et al. 2017). The humus enriched black soil (van Zomeren and Comans 2007) contains a large number of reducing functional groups, such as phenolic and hydroxylic groups (Chen et al. 2011; Hsu et al. 2009), and thus the Cr(VI) reduction reaction is still in progress (Zhang et al. 2018a). The breakthrough time of Cr(VI) in the black soil column is about 36 d, which indicates that the reduction of Cr(VI) in the soil column lasted for comparable time. In addition, the reduction of Cr(VI) was a hydrogen-consuming reaction (Reduction reactions is shown as follows, Equation 7, 8) (Huang et al. 2012). But the black soil contains a large amount of humus, which is rich in acidic functional groups, such as carboxylic groups and phenolic groups. These functional groups have strong pH buffering abilities. Thus, at the end of the experiment, the leachate pH of the black soil column remained at around 8.5 (lower than the pH in the red soil column which exceeded 10), which also allowed Cr(VI) to be reduced in the black soil column (Sillerova et al. 2014; Wittbrodt and Palmer 1995).

$$HCrO_4^- + 7H^+ + 3e^- \rightarrow Cr^{3+} + 4H_2O \quad (7)$$

$$Ar - O^{-}(phenol) \rightarrow Ar = O(carbonyl) + e^{-} \quad (8)$$

By observing Figure 2(b), it can be found that the outlet Cr(VI) concentration of the red soil column appears higher than the inlet concentration, which indicates that Cr(VI) adsorbed on the surface of the red soil desorbed. Because the alkaline Cr(VI) solution was continuously introduced into the red soil column, the acid-base balance of the red soil was broken. When the pH exceeded the PZC of red soil, the excess hydroxide competed for adsorption sites with Cr(VI), which is also the main reason for the over-estimation of the retention effect of red soil on Cr(VI). The same phenomena were observed in the sampling ports at 5 cm and 10 cm (Figure S5). The area of gray and reddish areas in Figure 2(b) is related to the adsorption amount and desorption amount of Cr(VI), respectively. Further observation shows that the areas of the two are almost equal, indicating that almost all adsorbed Cr(VI) was desorbed into the liquid phase. By comparing the adsorption and desorption amounts of Cr(VI) at the three sampling ports, which was calculated by the breakthrough curves (Figure S6), it can be found that the adsorbed Cr(VI) and desorbed Cr(VI) are all equivalent in quantity approximately. This further illustrates that the reversible adsorption acts as the retention mechanism of Cr(VI) on the red soil.

In addition, it can be observed in Figure S5(a) that the concentration of Cr(VI) leachate in the three sampling ports did not reach the initial concentration of Cr(VI). This indicates that there is always a liquid phase reduction process of Cr(VI) in the soil column, which may be caused by the redox reaction of dissolved organic matter in the liquid phase with Cr(VI).

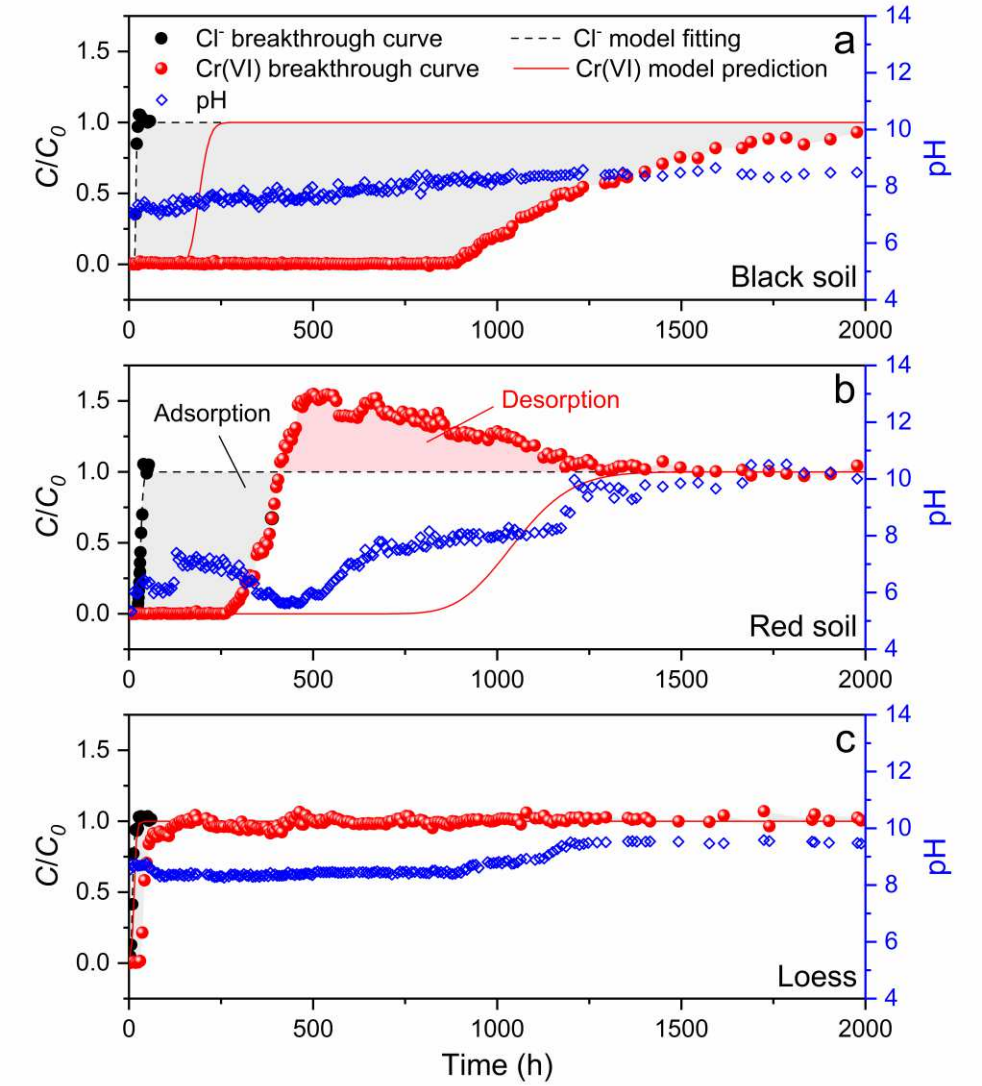

Figure 2. The dynamic transportation of Cr(VI) in the (a) black soil, (b) red soil and (c) loess columns. The initial Cr(VI) concentration was 100 mg L^{-1}. The initial pH of the inlet solution was 11.5. The background electrolyte was 0.02 M NaCl. The black dash line represents the breakthrough curve of Cl^- determined by convection-dispersion equation fitting. The red solid line represents the breakthrough curve of Cr(VI) determined by convection-dispersion equation prediction with the K_d obtained from the

isotherm model fitting. These curves correspond to the outlet of the column.

In order to verify the change of Cr content and speciation in the soil columns before and after the reaction, the soil column was divided into upper, middle and lower sections and analyzed by the BCR sequential extraction method, and the results are shown in Figure 3. It can be seen from the figure that the three soil samples contain a certain amount of Cr, which is the natural background content of Cr in the soil, mainly in the residual state and oxidizable state. And the content is between 30.38 and 71.76 mg kg^{-1}. The content of Cr in the red soil is the highest. After the reaction, the total content and speciation of Cr in red clay and loess almost kept unchanged. For the red soil, the desorption of Cr(VI) occurs after the pH of the solution changing to alkaline conditions. For the loess, it is mainly due to the weak adsorption of Cr(VI). It is worth noting that the content of Cr in the black soil after the reaction is significantly increased, and the Cr content decreases gradually as it approaches the outlet. From the change of speciation, the content of Cr in the oxidizable state is significantly increased, following by the Cr in the reducible state. These two forms represent Cr combined with soil organic matter and iron oxide, respectively. It can be seen that the speciation analysis results are consistent with the results of Cr(VI) breakthrough experiment.

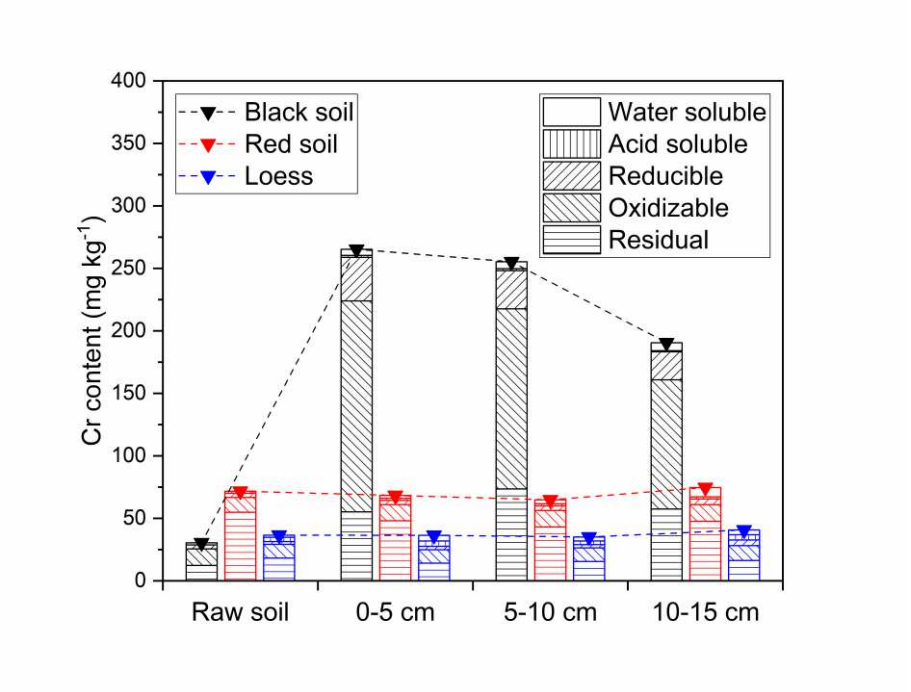

Figure 3. Cr speciation analysis results of black soil, red soil and loess before and after reaction.

In order to further clarify the valence state of Cr adsorbed on black soil, the black soil samples before and after the reaction were characterized by XPS Cr2p. The results are shown in Figure 4. It can be seen that the signal of Cr before the reaction is very weak, but the signal of Cr after the reaction is significantly enhanced. Through the peak fitting analysis, Cr(III) is dominated, accounting for 80.56% of the total Cr. It can be inferred that the majority of Cr(VI) adsorbed by black soil has been reduced, which is consistent with the speciation analysis results.

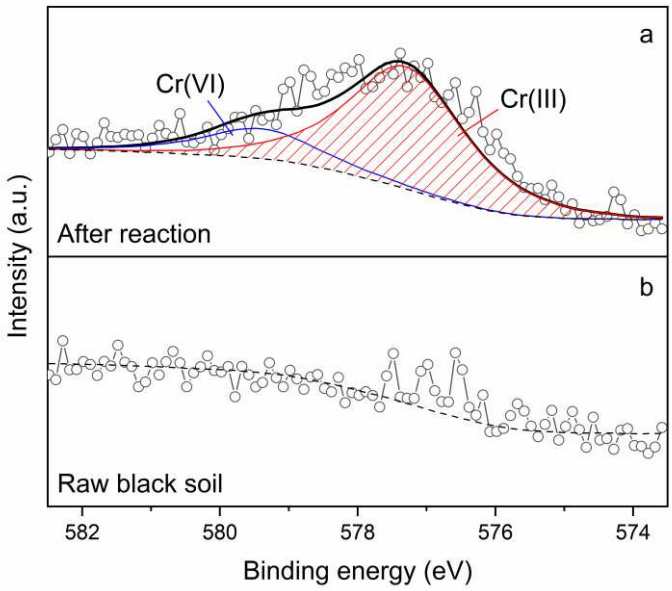

Figure 4. The XPS Cr2p determination of black soil sample before and after reaction(Soil near the inlet of the column). The dash line represents the baseline, and the blue and red line represent the Cr(VI) and Cr(III), respectively. The binding energy of Cr(VI) and Cr(III) were 579.4 (Elio et al. 1988) and 577.3 eV (Jianjun and Qunji 1994), respectively.

3.4 The implications for risk assessment and remediation

The pollution process and characteristics of the soil at COPR site are quite different from other Cr contaminated sites. Because the alkaline substances in the COPR can cause the alkalization of the soil, which will significantly affect the dynamic migration and transformation of Cr(VI) in soils. In this study, it was found that the red soil has strong adsorption capacity for Cr(VI) under natural soil pH conditions. However, almost all of the adsorbed Cr(VI) was desorbed as the soil pH increasing. This indicates that COPR site in the red soil area has strong environmental risks and should be given

enough attention. On the contrary, at the end of the experiment, the leaching solution pH of the black soil column reached about 8.5. The adsorption of Cr(VI) became weak, but the adsorption quantity of Cr(VI) in black soil was significant. And the adsorbed Cr(VI) didn't desorb till the end. The speciation analysis and XPS characterization results showed that the Cr in the black soil is mainly exist in the form of Cr(III), which indicates that Cr in the contaminated soil at the COPR site in the black soil area has low environmental risk. The environmental risk of Cr in soils is not only determined by the total amount of Cr, but also determined by the valence and existing form of Cr.

The current remediation projects of the contaminated soil in the COPR site in China mainly use inorganic reducing agent to reduce Cr(VI) to Cr(III), such as ferrous sulfate ($FeSO_4$) and calcium polysulfide (CaS_5) (Moon et al. 2008). However, the phenomenon of Cr(VI) re-release may occur in the remediation site (Moon et al. 2007). There are two reasons for this phenomenon. One is that the Cr(III) produced by reduction is unstable, which can be oxidized to Cr(VI) by the electron acceptors such as Mn oxides (Landrot et al. 2012a; Landrot et al. 2012b). The other is that the soil particles didn't contact with the inorganic reducing agent sufficiently, and the Cr(VI) inside the soil particles is not effectively reduced (Jagupilla et al. 2009). Additionally, the inorganic reducing agent is easily oxidized and deactivated in the air, so the Cr(VI) inside the soil particles is slowly released again. It can be seen that the remediation of Cr(VI) contaminated soils by using inorganic remediation agent is not stable. And the use of inorganic remediation agent may cause secondary pollution. In this study, it was found that the organic matter in black soil had a strong long-term reducing ability to Cr(VI),

which could effectively avoid the phenomenon of Cr(VI) re-release after remediation. In addition, soil organic matter can also provide complex adsorption sites for Cr(III) produced by reduction, which is not easy to desorb or oxidize, and greatly reduces the environmental risks of Cr in soil (Kožuh et al. 2000; Masscheleyn et al. 1992).

4 Conclusions

This study focused on the retardation process of the dynamic migration of Cr(VI) in leaching filtrate of COPR in different types of soils. It is found that the typical black soil, red soil and loess from different regions of China have great differences in the chemical composition and physicochemical properties. The red soil is rich in hematite, and Cr(VI) can be adsorbed on the hydroxyl sites on the surface of hematite by ligand exchange. The black soil is rich in organic matter, and the reducing functional group in the organic matter can slowly reduce Cr(VI) to Cr(III). Loess is an alkaline soil with low content of iron minerals and organic matter, and its adsorption capacity for Cr(VI) is poor. According to the results of dynamic migration column experiments, it can be found that the retardation effect of the loess on Cr(VI) migration is weak. The red soil has a strong adsorption capacity for Cr(VI), however, with the alkalization of the soil, the adsorbed Cr(VI) is re-desorbed, which will cause the strong environmental risk. Only black soil has a strong retardation effect on the migration of Cr(VI), indicating that organic matter is a potential environmentally friendly remediation material for Cr(VI) contaminated soils. On the one hand, organic matter can provide electrons for Cr(VI) reduction (Huang et al. 2012). On the other hand, organic matter can also offer additional hydrogen ions to provide favorable conditions for the hydrogen consuming

reduction of Cr(VI) (Zhang et al. 2018b). In order to give full play to the performance of organic matter on the adsorption and reduction of Cr(VI) in soils, the reduction mechanism of Cr(VI) by soil organic matter remains to be further revealed, such as the effect of the combination of soil organic matter and soil inorganic minerals for Cr(VI) adsorption and reduction, and the influence of soil microorganisms on the reduction of Cr(VI) by soil organic matter.

Acknowledgement

This work was financially supported by the National Natural Science Foundation of China (41977172), the National Key Research and Development Program of China (2020YFC1807002), and the Fundamental Research Funds for the Central Universities (2652019019).

Author contributions statement

Jia Zhang and Honghan Chen conceived the project. Minghai Wei wrote the main manuscript text with the help of Jia Zhang and Wenting Li. Wenting Li and Jie Tang participated in the main experiments. Minghai Wei performed the analysis and analyzed the data. All authors reviewed the manuscript.

Additional information

The authors declare no competing interests.

References

Adegoke HI, Adekola FA (2012) Equilibrium sorption of hexavalent chromium from aqueous solution using synthetic hematite Colloid Journal 74:420-426 doi:10.1134/s1061933x12040035

Barnie S, Zhang J, Wang H, Yin H, Chen H (2018) The influence of pH, co-existing ions, ionic strength, and temperature on the adsorption and reduction of hexavalent chromium by undissolved humic acid Chemosphere 212:209-218 doi:10.1016/j.chemosphere.2018.08.067

Benjamin MM (2002) Water Chemistry McGraw-Hill，New York

Bradl HB (2004) Adsorption of heavy metal ions on soils and soils constituents J Colloid Interface Sci 277:1-18 doi:10.1016/j.jcis.2004.04.005

Chen SY et al. (2011) Influence of chemical compositions and molecular weights of humic acids on Cr(VI) photo-reduction Journal of Hazardous Materials 197:337-344 doi:10.1016/j.jhazmat.2011.09.091

Choppala G, Bolan N, Lamb D, Kunhikrishnan A (2013) Comparative Sorption and Mobility of Cr(III) and Cr(VI) Species in a Range of Soils: Implications to Bioavailability Water Air and Soil Pollution 224 doi:10.1007/s11270-013-1699-6

Chrysochoou M, Fakra SC, Marcus MA, Moon DH, Dermatas D (2009) Microstructural analyses of Cr(VI) speciation in chromite ore processing residue (COPR) Environ Sci Technol 43:5461-5466 doi:10.1021/es9005338

Coleman D, Oades JM, Uehara G (1989) Dynamics of Soil Organic Matter in Tropical Ecosystems.

Dai W (2009) RELATIONSHIPS BETWEEN SOIL ORGANIC MATTER CONTENT(SOM) AND pH IN TOPSOIL OF ZONAL SOILS IN CHINA Acta Pedologica Sinica 46:851-860

Dhal B, Thatoi HN, Das NN, Pandey BD (2013) Chemical and microbial remediation

of hexavalent chromium from contaminated soil and mining/metallurgical solid waste: a review J Hazard Mater 250-251:272-291 doi:10.1016/j.jhazmat.2013.01.048

Elio D, Malitesta C, Zambonin P, Rivière J (1988) X-ray photoelectron spectroscopic study of some chromium-oxygen systems Surface and Interface Analysis 13:173-179 doi:10.1002/sia.740130210

Estes SL et al. (2013) A self-consistent model describing the thermodynamics of Eu(III) adsorption onto hematite Geochimica Et Cosmochimica Acta 122:430-447 doi:10.1016/j.gca.2013.08.023

Fendorf SE (1995) Surface reactions of chromium in soils and waters Geoderma 67:55-71 doi:https://doi.org/10.1016/0016-7061(94)00062-F

Fernandez-Pazos MT, Garrido-Rodriguez B, Novoa-Munoz JC, Arias-Estevez M, Fernandez-Sanjurjo MJ, Nunez-Delgado A, Alvarez E (2013) Cr(VI) Adsorption and Desorption on Soils and Biosorbents Water Air and Soil Pollution 224 doi:10.1007/s11270-012-1366-3

Foeldi C, Dohrmann R, Matern K, Mansfeldt T (2013) Characterization of chromium-containing wastes and soils affected by the production of chromium tanning agents Journal of Soils and Sediments 13:1170-1179 doi:10.1007/s11368-013-0714-2

Fonseca B, Teixeira A, Figueiredo H, Tavares T (2009) Modelling of the Cr(VI) transport in typical soils of the North of Portugal Journal of Hazardous Materials 167:756-762 doi:10.1016/j.jhazmat.2009.01.049

Gao Y, Xia J (2011) Chromium contamination accident in China: viewing environment

policy of China Environ Sci Technol 45:8605-8606 doi:10.1021/es203101f

Geelhoed JS, Meeussen JCL, Roe MJ, Hillier S, Thomas RP, Farmer JG, Paterson E (2003) Chromium Remediation or Release? Effect of Iron(II) Sulfate Addition on Chromium(VI) Leaching from Columns of Chromite Ore Processing Residue Environmental Science & Technology 37:3206-3213 doi:10.1021/es0264798

Gong Y-F, Song J, Ren H-T, Han X (2015) Comparison of Cr(VI) removal by activated sludge and dissolved organic matter (DOM): importance of UV light Environmental Science and Pollution Research 22:18487-18494 doi:10.1007/s11356-015-5182-3

He YT, Traina SJ (2005) Cr(VI) reduction and immobilization by magnetite under alkaline pH conditions: the role of passivation Environ Sci Technol 39:4499-4504 doi:10.1021/es0483692

Hsu N-H, Wang S-L, Lin Y-C, Sheng GD, Lee J-F (2009) Reduction of Cr(VI) by Crop-Residue-Derived Black Carbon Environmental Science & Technology 43:8801-8806 doi:10.1021/es901872x

Huang SW et al. (2012) Chromate reduction on humic acid derived from a peat soil - Exploration of the activated sites on HAs for chromate removal Chemosphere 87:587-594 doi:10.1016/j.chemosphere.2012.01.010

Jagupilla SC, Moon DH, Wazne M, Christodoulatos C, Kim MG (2009) Effects of particle size and acid addition on the remediation of chromite ore processing residue using ferrous sulfate Journal of Hazardous Materials 168:121-128 doi:10.1016/j.jhazmat.2009.02.012

James BR, Bartlett RJ (1983) Behavior of Chromium in Soils: VII. Adsorption and Reduction of Hexavalent Forms 1 J Environ Qual 12:177-181 doi:10.2134/jeq1983.00472425001200020005x

Jardine PM, Fendorf SE, Mayes MA, Larsen IL, Brooks SC, Bailey WB (1999) Fate and Transport of Hexavalent Chromium in Undisturbed Heterogeneous Soil Environmental Science & Technology 33:2939-2944 doi:10.1021/es981211v

Jiang J, Xu R, Wang Y, Zhao A (2008) The mechanism of chromate sorption by three variable charge soils Chemosphere 71:1469-1475 doi:10.1016/j.chemosphere.2007.12.012

Jiang W, Cai Q, Xu W, Yang M, Cai Y, Dionysiou DD, O'Shea KE (2014) Cr(VI) adsorption and reduction by humic acid coated on magnetite Environ Sci Technol 48:8078-8085 doi:10.1021/es405804m

Jianjun W, Qunji X (1994) Effects of synthetic additives on the friction and wear properties of a Cr2O3 coating Wear 176:213-216 doi:https://doi.org/10.1016/0043-1648(94)90149-X

Jin X, Jiang M, Du J, Chen Z (2014) Removal of Cr(VI) from aqueous solution by surfactant-modified kaolinite Journal of Industrial and Engineering Chemistry 20:3025-3032 doi:10.1016/j.jiec.2013.11.038

Johnston CP, Chrysochoou M (2012) Investigation of chromate coordination on ferrihydrite by in situ ATR-FTIR spectroscopy and theoretical frequency calculations Environ Sci Technol 46:5851-5858 doi:10.1021/es300660r

Johnston CP, Chrysochoou M (2014) Mechanisms of chromate adsorption on hematite

Geochimica Et Cosmochimica Acta 138:146-157 doi:10.1016/j.gca.2014.04.030

Johnston CP, Chrysochoou M (2015) Mechanisms of chromate adsorption on boehmite J Hazard Mater 281:56-63 doi:10.1016/j.jhazmat.2014.05.067

Johnston CP, Chrysochoou M (2016) Mechanisms of Chromate, Selenate, and Sulfate Adsorption on Al-Substituted Ferrihydrite: Implications for Ferrihydrite Surface Structure and Reactivity Environ Sci Technol 50:3589-3596 doi:10.1021/acs.est.5b05529

Klingenfuss C, Rosskopf N, Walter J, Heller C, Zeitz J (2014) Soil organic matter to soil organic carbon ratios of peatland soil substrates Geoderma 235:410-417 doi:10.1016/j.geoderma.2014.07.010

Knorr B, Maloszewski P, Kraemer F, Stumpp C (2016) Diffusive mass exchange of non-reactive substances in dual-porosity porous systems - column experiments under saturated conditions Hydrological Processes 30:914-926 doi:10.1002/hyp.10620

Kožuh N, Štupar J, Gorenc B (2000) Reduction and Oxidation Processes of Chromium in Soils Environmental Science & Technology 34:112-119 doi:10.1021/es981162m

Landrot G, Ginder-Vogel M, Livi K, Fitts JP, Sparks DL (2012a) Chromium(III) Oxidation by Three Poorly-Crystalline Manganese(IV) Oxides. 1. Chromium(III)-Oxidizing Capacity Environmental Science & Technology 46:11594-11600 doi:10.1021/es302383y

Landrot G, Ginder-Vogel M, Livi K, Fitts JP, Sparks DL (2012b) Chromium(III)

Oxidation by Three Poorly Crystalline Manganese(IV) Oxides. 2. Solid Phase Analyses Environmental Science & Technology 46:11601-11609 doi:10.1021/es302384q

Lee SZ, Chang L, Ehrlich R (1999) The relationship between adsorption of Cr(VI) and soil properties Journal of Environmental Science & Health Part A A34:809-833 doi:10.1080/10934529909376867

Ma J, Wang Z, Gao Y, Yang Q, Chen J, Chen Y, Xie Y (2013) BCR Speciation Analysis of Lead in Yunnan Red Soil. In: Yu L, Guo J, Yi G, Yu Q (eds) Advances in Chemical Engineering Iii, Pts 1-4, vol 781-784. Advanced Materials Research. pp 2315-+. doi:10.4028/www.scientific.net/AMR.781-784.2315

Masscheleyn PH, Pardue JH, DeLaune RD, Patrick JWH (1992) Chromium Redox Chemistry in a Lower Mississippi Valley Bottomland Hardwood Wetland Environmental Science & Technology 26:1217-1226 doi:10.1021/es50002a611

Moon DH et al. (2007) Long-term treatment issues with chromite ore processing residue (COPR): Cr6+ reduction and heave Journal of Hazardous Materials 143:629-635 doi:10.1016/j.jhazmat.2007.01.013

Moon DH, Wazne M, Jagupilla SC, Christodoulatos C, Kim MG, Koutsospyros A (2008) Particle size and pH effects on remediation of chromite ore processing residue using calcium polysulfide (CaS5) Sci Total Environ 399:2-10 doi:10.1016/j.scitotenv.2008.03.040

Moussout H, Ahlafi H, Aazza M, Maghat H (2018) Critical of linear and nonlinear equations of pseudo-first order and pseudo-second order kinetic models Karbala

International Journal of Modern Science 4:244-254 doi:https://doi.org/10.1016/j.kijoms.2018.04.001

Nakato T, Kawamata J, Takagi S (2017) Inorganic Nanosheets and Nanosheet-Based Materials Springer Japan 10.1007/978-4-431-56496-6

Saha R, Nandi R, Saha B (2011) Sources and toxicity of hexavalent chromium Journal of Coordination Chemistry 64:1782-1806 doi:10.1080/00958972.2011.583646

Sijin L, Wenfeng T, Fan L (2006) Point of zero charge (PZC) of manganese oxides determined with an improved salt titration method Acta Pedologica Sinica 43:756-763 doi:10.1016/S1872-2032(06)60050-4

Sillerova H, Chrastny V, Cadkova E, Komarek M (2014) Isotope fractionation and spectroscopic analysis as an evidence of Cr(VI) reduction during biosorption Chemosphere 95:402-407 doi:10.1016/j.chemosphere.2013.09.054

Singh DB, Gupta GS, Prasad G, Rupainwar DC (1993) The Use of Hematite for Chromium(VI) Removal Journal of Environmental Science and Health Part A: Environmental Science and Engineering and Toxicology 28:1813-1826

Toride N, Leij F, Van Genuchten M (1995) The CXTFIT Code for Estimating Transport Parameters from Laboratory or Field Tracer Experiments Salinity Laboratory 137

van Zomeren A, Comans RNJ (2007) Measurement of Humic and Fulvic Acid Concentrations and Dissolution Properties by a Rapid Batch Procedure Environmental Science & Technology 41:6755-6761 doi:10.1021/es0709223

Wang Y, Yang Z, Chai L, Zhao K (2009) Diffusion of hexavalent chromium in chromium-containing slag as affected by microbial detoxification Journal of

Hazardous Materials 169:1173-1178 doi:10.1016/j.jhazmat.2009.04.060

Wang Z-x, Chen J-q, Chai L-y, Yang Z-h, Huang S-h, Zheng Y (2011) Environmental impact and site-specific human health risks of chromium in the vicinity of a ferro-alloy manufactory, China Journal of Hazardous Materials 190:980-985 doi:10.1016/j.jhazmat.2011.04.039

Weng CH, Huang CP, Allen HE, Cheng AHD, Sanders PF (1994) Chromium Leaching Behavior in Soil Derived from Chromite Ore Processing Waste Sci Total Environ 154:71-86 doi:10.1016/0048-9697(94)90615-7

Weng L, Temminghoff EJ, Lofts S, Tipping E, Van Riemsdijk WH (2002) Complexation with dissolved organic matter and solubility control of heavy metals in a sandy soil Environ Sci Technol 36:4804-4810 doi:10.1021/es0200084

Wittbrodt PR, Palmer CD (1995) Reduction of Cr(VI) in the Presence of Excess Soil Fulvic Acid Environmental Science & Technology 29:255-263 doi:10.1021/es00001a033

Xie JY, Gu XY, Tong F, Zhao YP, Tan YY (2015) Surface complexation modeling of Cr(VI) adsorption at the goethite-water interface J Colloid Interface Sci 455:55-62 doi:10.1016/j.jcis.2015.05.041

Žemberyová M, Bartekova J, Hagarova I (2006) The utilization of modified BCR three-step sequential extraction procedure for the fractionation of Cd, Cr, Cu, Ni, Pb and Zn in soil reference materials of different origins Talanta 70:973-978 doi:10.1016/j.talanta.2006.05.057

Zhang J, Chen L, Yin H, Jin S, Liu F, Chen H (2017) Mechanism study of humic acid

functional groups for Cr(VI) retention: Two-dimensional FTIR and C-13 CP/MAS NMR correlation spectroscopic analysis Environmental Pollution 225:86-92 doi:10.1016/j.envpol.2017.03.047

Zhang J, Yin H, Barnie S, Wei M, Chen H (2019a) Mechanism and modeling of hexavalent chromium interaction with a typical black soil: the importance of the relationship between adsorption and reduction Electronic supplementary information (ESI) available. See DOI: 10.1039/c8ra08154a Rsc Advances 9:5582-5591 doi:10.1039/c8ra08154a

Zhang J, Yin H, Chen L, Liu F, Chen H (2018a) The role of different functional groups in a novel adsorption-complexation-reduction multi-step kinetic model for hexavalent chromium retention by undissolved humic acid Environmental Pollution 237:740-746 doi:10.1016/j.envpol.2017.10.120

Zhang J et al. (2019b) Molecular structure-reactivity correlations of humic acid and humin fractions from a typical black soil for hexavalent chromium reduction Science of the Total Environment 651:2975-2984 doi:10.1016/j.scitotenv.2018.10.165

Zhang J, Yin H, Wang H, Xu L, Samuel B, Liu F, Chen H (2018b) Reduction mechanism of hexavalent chromium by functional groups of undissolved humic acid and humin fractions of typical black soil from Northeast China Environmental Science and Pollution Research 25:16913-16921 doi:10.1007/s11356-018-1878-5

Zhang J, Yin HL, Samuel B, Liu F, Chen HH (2018c) A novel method of three-dimensional hetero-spectral correlation analysis for the fingerprint identification

of humic acid functional groups for hexavalent chromium retention RSC Adv 8:3522-3529 doi:10.1039/c7ra12146f

Figures

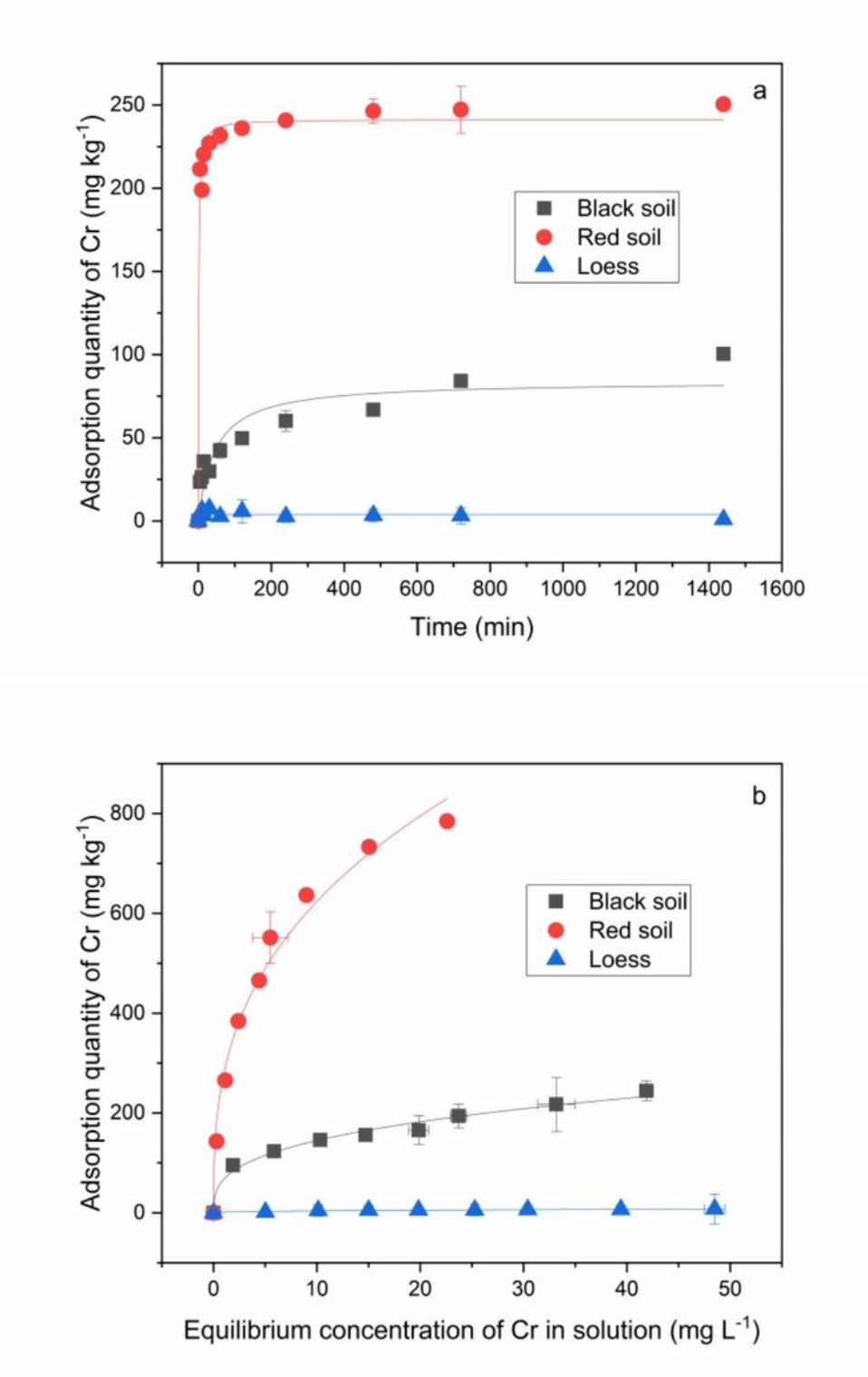

Figure 1

The (a) kinetic and (b) thermodynamic characteristics of Cr(VI) adsorption by black soil, red soil and loess samples at 25 °C. The initial pH of Cr(VI) solution was 6.5, and the background electrolyte was 0.02 M NaCl. The error bar represented Standard Error of Mean. In kinetic experiments, the simulation results

were more consistent with the pseudo second-order reaction kinetic model. The solid lines are Freundlich isotherm in (b).

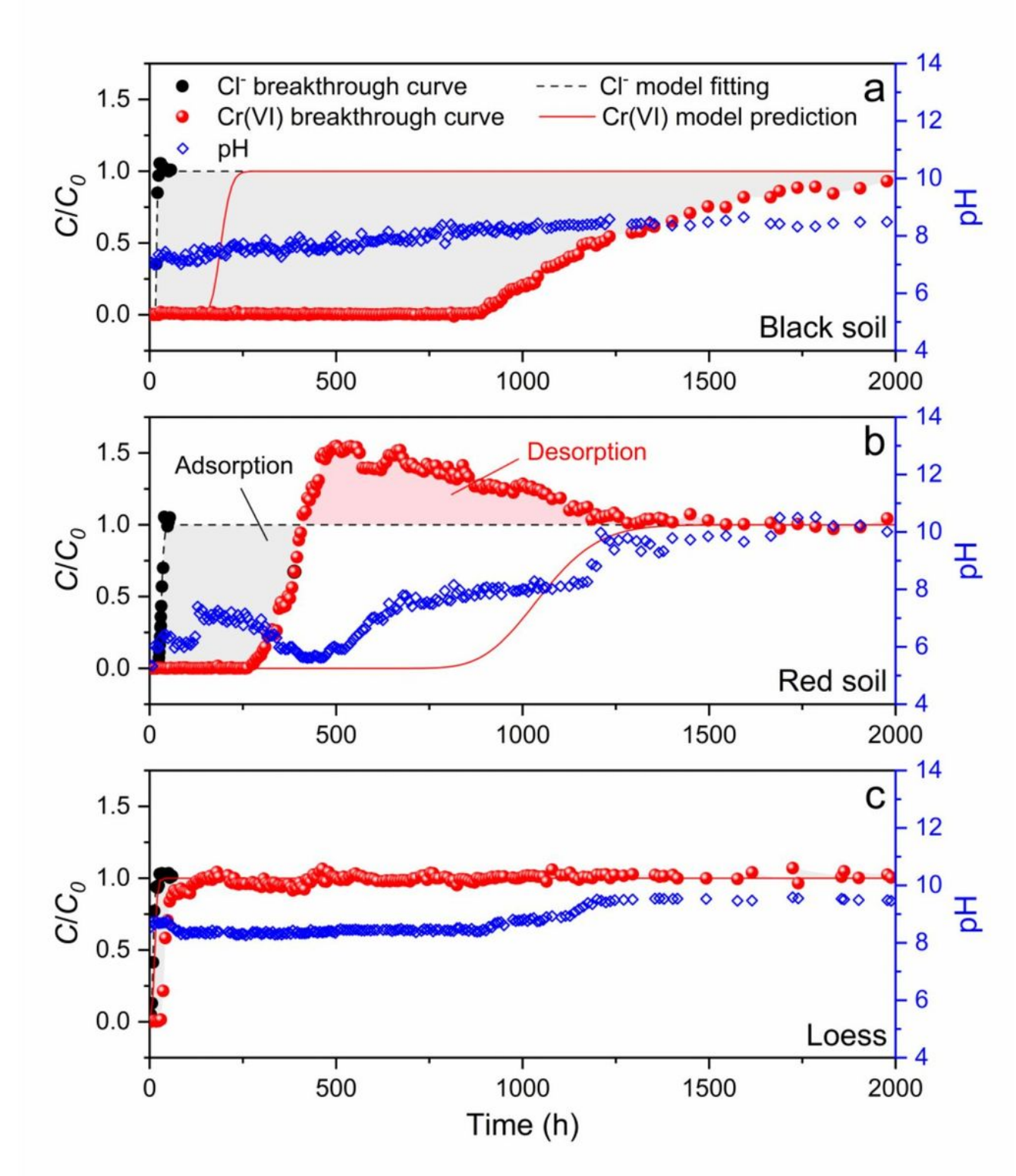

Figure 2

The dynamic transportation of Cr(VI) in the (a) black soil, (b) red soil and (c) loess columns. The initial Cr(VI) concentration was 100 mg L-1. The initial pH of the inlet solution was 11.5. The background electrolyte was 0.02 M NaCl. The black dash line represents the breakthrough curve of Cl- determined by

convection-dispersion equation fitting. The red solid line represents the breakthrough curve of Cr(VI) determined by convection-dispersion equation prediction with the Kd obtained from the isotherm model fitting. These curves correspond to the outlet of the column.

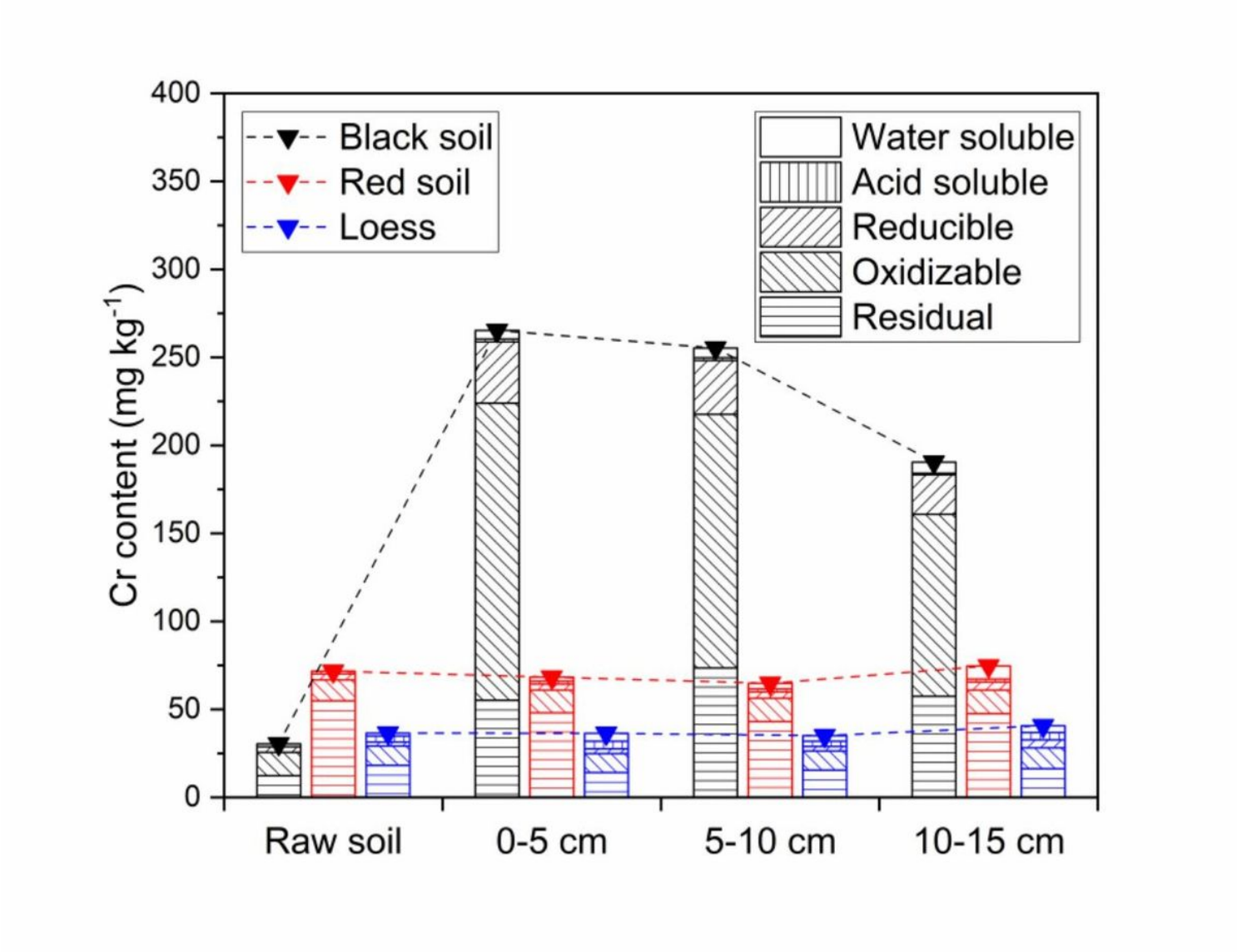

Figure 3

Cr speciation analysis results of black soil, red soil and loess before and after reaction.

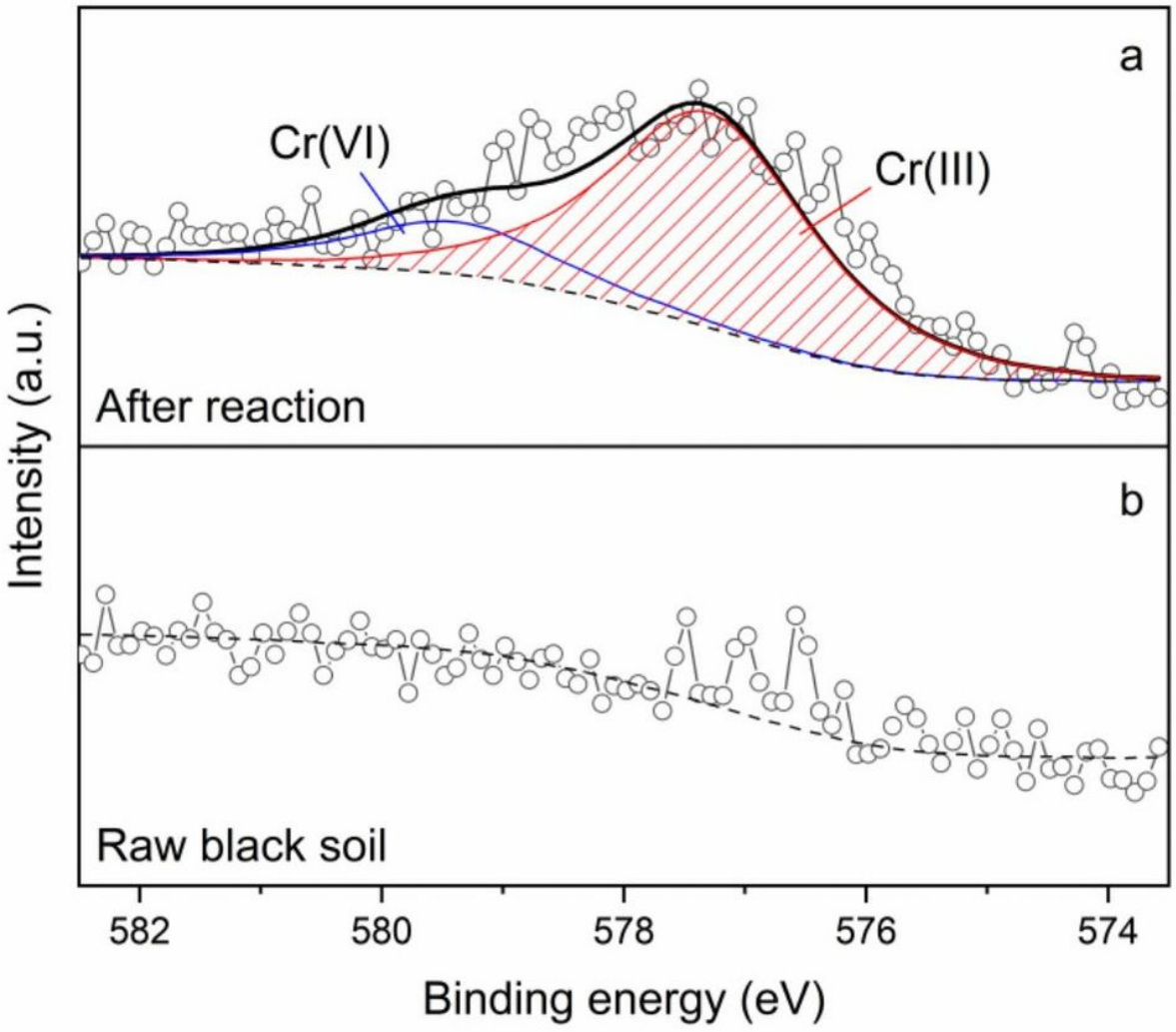

Figure 4

The XPS Cr2p determination of black soil sample before and after reaction(Soil near the inlet of the column). The dash line represents the baseline, and the blue and red line represent the Cr(VI) and Cr(III), respectively. The binding energy of Cr(VI) and Cr(III) were 579.4 (Elio et al. 1988) and 577.3 eV (Jianjun and Qunji 1994), respectively.

Supplementary Files

This is a list of supplementary files associated with this preprint. Click to download.

- SupplementaryInformation.docx